



POTSDAM-INSTITUT FÜR  
KLIMAFOLGENFORSCHUNG



**Originally published as:**

Sunny, E. M., Balakrishnan, J., [Kurths, J.](#) (2023): Predicting climatic tipping points. - Chaos, 33, 2, 021101.

DOI: <https://doi.org/10.1063/5.0135266>

RESEARCH ARTICLE | FEBRUARY 06 2023

## Predicting climatic tipping points

Eros M. Sunny ; Janaki Balakrishnan  ; Jürgen Kurths 



Chaos 33, 021101 (2023)

<https://doi.org/10.1063/5.0135266>



CrossMark



**APL Machine Learning**  
**Latest Articles Online!**  
**Read Now**



# Predicting climatic tipping points

Cite as: Chaos 33, 021101 (2023); doi: 10.1063/5.0135266

Submitted: 17 November 2022 · Accepted: 9 January 2023 ·

Published Online: 6 February 2023



View Online



Export Citation



CrossMark

Eros M. Sunny,<sup>1,a)</sup>  Janaki Balakrishnan,<sup>1,b)</sup>  and Jürgen Kurths<sup>2</sup> 

## AFFILIATIONS

<sup>1</sup>School of Natural Sciences and Engineering, National Institute of Advanced Studies (NIAS), Indian Institute of Science Campus, Bangalore 560012, India

<sup>2</sup>Potsdam Institute for Climate Impact Research, PO Box 601203, Potsdam 14412, Germany

<sup>a)</sup>**Current address:** Department of Mathematics, Little Hall 358, University of Florida, Gainesville, FL 32611, USA.

<sup>b)</sup>**Author to whom correspondence should be addressed:** [janaki05@gmail.com](mailto:janaki05@gmail.com)

## ABSTRACT

Increased levels of greenhouse gases in the atmosphere, especially carbon dioxide, are leading contributors to a significant increase in the global temperature, and the consequent global climatic changes are more noticeable in recent years than in the past. A persistent increased growth of such gases might lead to an irreversible transition or tipping of the Earth's climatic system to a new dynamical state. A change of regimes in CO<sub>2</sub> buildup being correlated to one in global climate patterns, predicting this tipping point becomes crucially important. We propose here an innovative conceptual model, which does just this. Using the idea of rate-induced bifurcations, we show that a sufficiently rapid change in the system parameters beyond a critical value tips the system over to a new dynamical state. Our model when applied to real-world data detects tipping points, enables calculation of tipping rates and predicts their future values, and identifies thresholds beyond which tipping occurs. The model well captures the growth in time of the total global atmospheric fossil-fuel CO<sub>2</sub> concentrations, identifying regime shift changes through measurable parameters and enabling prediction of future trends based on past data. Our model shows two distinct routes to tipping. We predict that with the present trend of variation of atmospheric greenhouse gas concentrations, the Earth's climatic system would move over to a new stable dynamical regime in the year 2022. We determine a limit of 10.62 GtC at the start of 2022 for global CO<sub>2</sub> emissions in order to avoid this tipping.

Published under an exclusive license by AIP Publishing. <https://doi.org/10.1063/5.0135266>

The Earth's climate has seen many changes over the years, affecting the physical environment (be it terrestrial, marine, or the atmosphere). These major changes or regime shifts from one stable dynamical state of the physical environment to another, each of which may persist for several years, produce major shifts in natural ecosystems involving trophic structures, changes in composition, and abundance of species. The climatic system moves over to a new regime once it crosses a climatic tipping point—a threshold crossed irreversibly by the system's dynamics. Anthropogenic influences brought about in the physical environment invariably contribute in a substantial way to climate change globally as the dynamics of the climatic system is governed by the coupling between the land, the atmosphere, and the oceans. An increase in levels of greenhouse gases in the atmosphere mainly caused by human activities, especially carbon dioxide, has been one of the important contributing factors leading to climate change in the last few decades. We present here a theoretical model that well captures the rate of increase of the total global

concentrations of carbon dioxide, the major contributing greenhouse gas in the atmosphere. We then employ the concept of rate-induced bifurcations to demonstrate that it is possible to determine the climatic tipping points from our model. This way, we predict that the climatic system would relocate to a new stable state early in the year 2022. It has been widely accepted that tipping point mechanisms can be used to study climate change. In this paper, we shall introduce and apply a rate-induced tipping model to global fossil-fuel emissions data. Our model shows two distinct routes in which tipping can occur, and the parameters describing these can be calculated from data and are physically measurable. Through the application of this model, we identify crucial tipping points, which lead to climate change and quantify exact boundaries crossed that induce tipping. Control can be exercised over the parameters describing tipping, if desired, such that tipping can be prevented. The methods developed can further be applied to any growth curve that may have undergone rate-induced tipping.

## I. INTRODUCTION

Technological advances over the years, especially with the advent of the industrial revolution, have been synonymous with increasing measures of fuel consumption and the consequent release into the atmosphere of the by-products of their burning. Global carbon dioxide concentrations in the atmosphere have drastically increased by an order of magnitude between 1926 and 2014 due to burning of fossil fuels. In the four decades between 1970 and 2014, the carbon dioxide concentration increased about 2.43 times, while  $\text{NO}_x$  and methane concentrations rose by about 2 and 1.8 times, respectively. Global temperatures have consequently risen considerably, and climatic conditions globally have changed compared to past years accompanied by rising sea levels. The Earth has also seen declining levels of Arctic sea ice and declining mass of land ice sheets in Greenland and Antarctica. Changes in natural ecosystems—both terrestrial and marine, change of habitat of fauna and flora, changed patterns of insect pest outbreak cycles, etc.—have been observed, and these are believed to have occurred as a consequence of the changed climate.<sup>1–4</sup>

It is, thus, of extreme interest and importance to know whether and when the next drastic change in the climate is likely to occur. If the rate of variation in concentrations of greenhouse gases in the atmosphere continued to follow the present trend, could one predict when Earth's climatic system would tip over irreversibly to a new dynamical state?

We propose here a theoretical model for the variation in the concentrations of the greenhouse gases in the atmosphere. We assume that the growth rate of the substance in the atmosphere and the carrying capacity for the gas are not constant but evolve in time. Using the concept of rate-induced bifurcations, we then show that a sufficiently rapid change in the system parameters beyond a critical value causes the system to tip or move away from a branch of attractors taking the system to a new dynamical state. We apply our theoretical model to recorded data of  $\text{CO}_2$  emissions available in<sup>5</sup> and compare it with the available global temperature anomaly data. We find that our theory matches very well with climatic tipping point years interpreted in the literature from observations of various natural ecosystems. We then predict that with the present trend of variation of greenhouse gas concentrations in the atmosphere, the Earth's climatic system would move over to a new stable dynamical regime in the year 2022.

While climatic regime shifts may best be described and understood using global climate models, such as general circulation models,<sup>6–8</sup> fluxes and transport of carbon dioxide and other gases, including other greenhouse gases between the atmosphere, land, and ocean are also affected by the changing climate. In our work, we introduce a conceptual model and a systematic procedure to study the growth of atmospheric fossil-fuel  $\text{CO}_2$  and to identify regime shift changes in it, which we posit are also climatic regime shifts.

The growth of carbon dioxide and other greenhouse gases, such as methane and nitrous oxide, which are by-products of human lifestyle and needs, is continually changing and is limited only by the changing technologies. One of the most popular choices to model a growth process is the logistic equation used in various disciplines because of its simplicity and practicality. Since the growth rate of the concentration of these gases in the atmosphere is not vanishing, their respective carrying capacities are not constants but time-varying.

A general form of this equation is the following:

$$\frac{dN}{dt} = A_0 + rN \left( 1 - \frac{N}{K} \right),$$

having two non-zero fixed points:  $N^* = \frac{Kr \pm K\sqrt{r^2 + 4\frac{r}{K}A_0}}{2r}$  with the smaller value of  $N^*$  being unstable and the other being stable. We will use this logistic equation augmented with a shift in the parameters to fit the growth curve of global  $\text{CO}_2$  emissions from fossil fuels and analyze tipping points.

Tipping happens when a system undergoes a dramatic change from one state to another new stable state.<sup>9,10</sup>

In our system, we observe two different ways in which tipping can occur. One is a rate-induced tipping (defined to occur when there is failure to follow a quasi-equilibrium state, which happens due to rapidly varying parameters) and the second is when  $\text{CO}_2$  levels exceed a certain threshold.

The first type of tipping happens when the rate of change in the parameters of the system is too high. Suppose we have a stable state and now, we allow the parameters of the system to change. Then, the stable state will also change along with the parameters. However, if the change is too fast, the system will not be able to keep up with the changing parameters and fails to track its quasi-equilibrium state, leading to rate-induced tipping. In our system, the parameter  $\mu$ , the speed of the shift of the equilibria, describes this.

Ashwin *et al.*<sup>11</sup> discussed rate-induced tipping and how it could be a possible mechanism for studying regime changes in climate systems. Building on this work, Ritchie and Sieber<sup>12</sup> analyzed a simple model for rate-induced tipping and early warning indicators for this.

We, however, consider a more complicated system inspired from a time-dependent logistic growth model augmented with a shift in parameters, which is shown to have two distinct ways of tipping. The parameters related to these tipping mechanisms are measurable and physically significant. In fact, the model quantifies exact boundaries, which need to be crossed for tipping to happen. This allows control over tipping by control over these parameters.

Our model is then applied to a real-world system—fossil-fuel  $\text{CO}_2$  emissions. The model helps to identify the points of the regime shift (tipping points) and calculates important measurable parameters ( $\mu$ ,  $N_{\text{transition}}$ ), which help in controlling the future growth and tipping of the system. We also point out a possible correlation between the regime shift years we calculated and changes in certain important climate parameters, such as the global temperature anomaly and a parameter we introduce associated with the ocean carbon sink.

The second type of tipping happens in our system only when the first has occurred. In our system, there are four fixed points: one of which is a sink, two are saddles, and one is a source. The sink has a basin of attraction. However, if an initial point, i.e.,  $N_{\text{transition}}$  is outside the basin, then no growth to the next stable state will occur. It will be shown that an explicit condition on  $N_{\text{transition}}$  may be obtained by which tipping may be prevented.

In short, our system has two parameters describing two different ways of tipping. These two parameters can be calculated from data and are measurable. Thus, tipping can be prevented, if desired, by controlling these parameters.

## II. THE MODEL

Greenhouse gas emissions, and among these, carbon dioxide, in particular, are known to be the main contributors to global temperature rise and a consequent climate change. We intend to model the growth of atmospheric carbon dioxide from fossil-fuel emissions and based on the premise that climate change is primarily driven by this growth curve and to understand the dynamical mechanisms through which climatic tipping to a new stable state occurs.

A careful analysis (see Appendix A) of the recorded data from Ref. 5 (Fig. 1, purple dots) shows that the growth in the global CO<sub>2</sub> fossil-fuel emissions occurs in certain phases. This prompts us to model this growth with the following system of equations:

$$\frac{dN}{dt} = A_0(t) + r(t)N \left( 1 - \frac{N}{K(t)} \right), \quad (1a)$$

$$\frac{d\lambda}{dt} = \mu\lambda(1 - \lambda), \quad (1b)$$

where  $N$  denotes CO<sub>2</sub> emissions from fossil-fuel in the atmosphere, with the growth rate  $r$  and the carrying capacity  $K$ , its growth being governed by a time-dependent generalized logistic equation. The time-varying parameter  $A_0(t)$  is usually negative and brings down the gas concentration—accounting, thereby, for the carbon sink. We assume that  $A_0$ ,  $K$ , and  $r$  are step functions of time and that they vary together, i.e., when  $r(t)$  changes its value, so must  $K(t)$  and  $A_0(t)$ . The real time variation of these parameters may be abrupt but continuous, and a step function approximation here is easier to work with as the parameters are constant on a given time interval. The variations of the parameters  $A_0(t)$ ,  $r(t)$ , and  $K(t)$  are set by  $A_0(t) = a_0 + a_1\lambda(t)$ ,  $r(t) = r_0 + r_1\lambda(t)$ ,  $K(t) = k_0 + k_1\lambda(t)$  ( $a_0, a_1, r_0, r_1, k_0$  and  $k_1$  are constants and  $r(t) > 0$ ,  $K(t) > 0$ , and  $\mu > 0$  are constraints we add for the sake of physical interpretation). Thus, our system of Eqs. (1a) and (1b) can be explicitly written as

$$\frac{dN}{dt} = a_0 + a_1\lambda(t) + (r_0 + r_1\lambda(t))N \left( 1 - \frac{N}{(k_0 + k_1\lambda(t))} \right), \quad (2a)$$

$$\frac{d\lambda}{dt} = \mu\lambda(1 - \lambda). \quad (2b)$$

$\lambda$  varies in time in the form of a ramp, which we model with its smoothed approximation, the logistic function [Eq. (1b)]. This models the growth when the parameters change as step functions of time,

$$\lambda(t) = \frac{1}{2} \left[ \tanh \left( \frac{\mu t}{2} \right) + 1 \right], \quad (3)$$

where the quantity  $\mu$  is the speed of the ramp-like shift in time of the parameters. We emphasize that we choose this functional form for the variation of the parameters for the sake of simplicity. We need only to consider the behavior of the system in the domain  $\mathcal{D} = [0, 1] \times \mathbb{R}$ .

In Fig. 2, we depict how  $N$  and the parameters in the system vary in time. We refer to a *period of growth* as that which corresponds to the growth of  $N$ , while the parameters ( $r, K, A_0$ ) remain approximately constant. The parameters vary in a *transition period*.

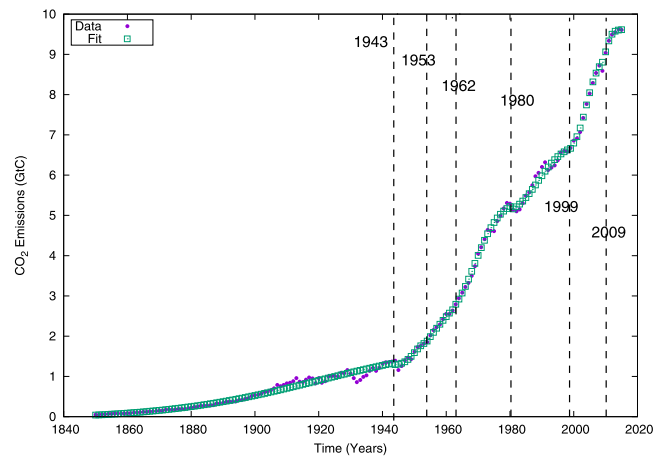


FIG. 1. Growth in time  $t$  of CO<sub>2</sub> emissions from fossil fuels in the atmosphere,  $N$  from recorded data (purple dots), and as calculated from our model (green squares). Dashed vertical lines show tipping/transition years as obtained from our model.

This period, corresponding to the growth of the parameters, contains two periods of growth of  $N$ . The speed  $\mu$  of the variation of the parameters or the shift of the equilibria of  $N$  is calculated from one transition period. We refer to the transition point as one where the second period of growth starts in a transition phase. We define these terms below.

**Definitions.** *Period of growth:* A period of growth is a period of time where a growth of  $N$  occurs, but the parameters  $r, K, A_0$  are assumed to be approximately constant.

*Transition phase:* A transition phase consists of two adjacent periods of growth put together. There is growth in  $N$  and a change of parameters in a transition phase.

*Transition point:* The value of  $t$  in one transition period at which the derivatives of the parameters take the maximum value.

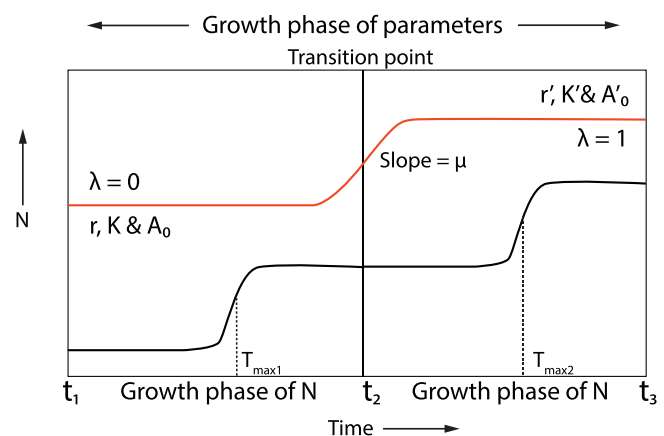
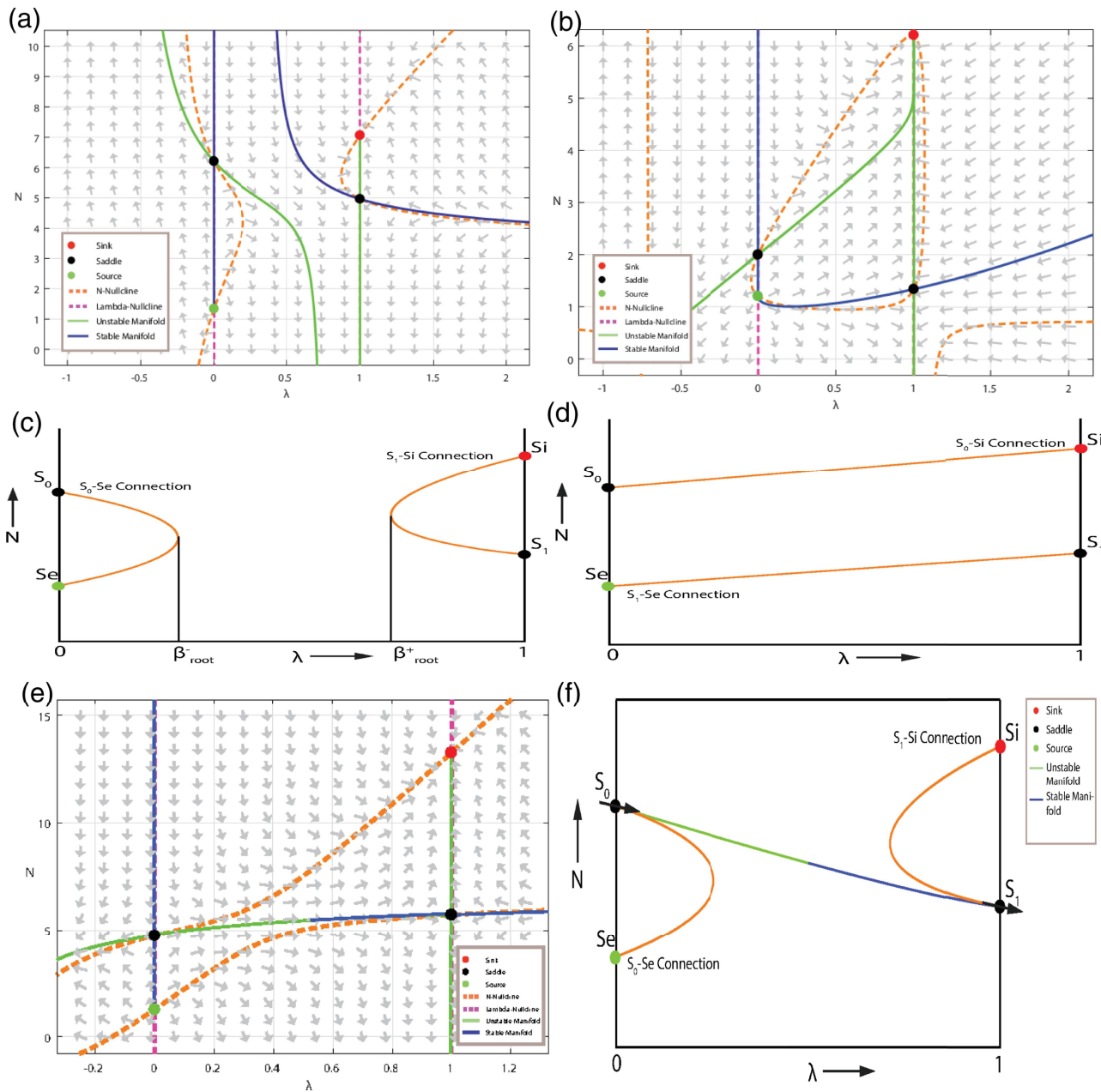


FIG. 2. Illustration of a transition.



**FIG. 3.** How the model works: (a) admissible phase portrait,  $\mu$  small; (b) non-admissible phase portrait; (c)  $S_0$ - $S_e$  and  $S_1$ - $S_i$  connections; (d)  $S_0$ - $S_i$  and  $S_1$ - $S_e$  connections; (e) non-admissible phase portrait with a saddle-saddle connection, parameter values:  $r_0 = r_1 = 1, a_0 = -1, a_1 = -7, k_0 = 6, k_1 = 13$ ; and (f) saddle-saddle connection at  $\mu_c$ .

$T_{\max}$  is the value of  $t$  in one period of growth at which  $\frac{dN}{dt}$  attains its maximum value (see also Appendix A). The solution of Eqs. (1a) and (1b) in one period of growth where the parameters are assumed to be constant is given in Eq. (A1) of Appendix A.

The plot depicted in Fig. 1 (green squares) of the measured  $CO_2$  atmospheric fossil fuel concentrations and those calculated

from our Eqs. (1a) and (1b) demonstrates that our model captures almost exactly their growth in time. The parameters are found as described in Appendix A. This enables us to identify the stable and unstable fixed points of the system; Eq. (1b) describes the rate of shift of the quasi-equilibrium states of the system.

Our next task is to identify critical  $\mu$ , which determines the future growth (as in Ref. 12) and beyond which the process of transition to a new state is set into motion.

Our system is much more complicated, but it can undergo rate-induced tipping by the same mechanism as in Ref. 12.

As described there, a *saddle–saddle connection is what defines our rate-induced tipping point.*

However, owing to the complexity of our system, such saddle–saddle connections are present only under certain conditions. It may be noted (from Peixoto's theorem) that our system with a saddle–saddle connection is not structurally stable.

Section II A, Secs. III A–III F, and Appendixes A–G deal with mathematically examining the system defined in Eqs. (1a) and (1b).

### A. Saddle–saddle connections in the system

Figures 3(a) and 3(b) show two phase portraits of the system (1a) and (1b) for two sets of parameters. We shall prove a theorem that shows why the first phase portrait has a saddle–saddle connection, while the second does not. Two important properties of the first phase portrait that allows it to have a saddle–saddle connection are as follows:

1. The  $N$  nullclines (dashed curves in orange) do not exist for a certain values of  $\lambda$ .
2. The saddle on  $\lambda = 1$  sits below the saddle on  $\lambda = 0$ . Note that  $\lambda \in [0, 1]$ , and therefore, we need not consider the behavior of the phase portrait in regions other than  $\lambda \in [0, 1]$ .

Here, we introduce some notation, which we shall be using throughout the paper.

#### Notation.

$S_0$  and  $S_1$ : These denote the saddles on  $\lambda = 0$  and  $\lambda = 1$ , respectively.

$S_i$  and  $S_e$ : These denote the sink and the source, respectively.

$S_1$ – $S_e$  connection: The  $N$  nullcline connection  $S_1$  to  $S_e$  (if it exists) is called a  $S_1$ – $S_e$  connection.

$S_1$ – $S_i$  connection: The  $N$  nullcline connection  $S_1$  to  $S_i$  (if it exists) is called a  $S_1$ – $S_i$  connection.

$S_0$ – $S_i$  connection: The  $N$  nullcline connection  $S_0$  to  $S_i$  (if it exists) is called a  $S_0$ – $S_i$  connection.

$S_0$ – $S_e$  connection: The  $N$  nullcline connection  $S_0$  to  $S_e$  (if it exists) is called a  $S_0$ – $S_e$  connection. These connections are depicted in Figs. 3(c) and 3(d).

$N(P)$ : Denotes the  $N$  coordinate of a point  $P$ .

$\Delta m := N(S_1) - N(S_0)$ .

We let  $m_0 = N(S_0)$  and  $m_1 = N(S_1)$ .

We find it useful to define two kinds of phase portraits, which the system exhibits.

#### Admissible phase portrait

A phase portrait with four fixed points and a  $S_1$ – $S_i$  connection, but no  $S_1$ – $S_e$  connection is called an admissible phase portrait [Fig. 3(a)].

#### Non-admissible phase portrait

A phase portrait that is not admissible [Fig. 3(b)].

We state below a theorem (proved in Appendixes B and C), which we shall use to locate tipping points of the climatic system

from the CO<sub>2</sub> growth curve. The theorem gives conditions for the system to admit a saddle–saddle connection for some finite  $\mu$ .

**Theorem.** *The following system:*

$$\frac{d\lambda}{dt} = \mu\lambda(1 - \lambda), \quad (4)$$

$$\frac{dN}{dt} = A_0(t) + r(t)N - \frac{r(t)}{K(t)}N^2, \quad (5)$$

where  $A_0(t) = a_0 + a_1\lambda(t)$ ,  $r(t) = r_0 + r_1\lambda(t)$ ,  $K(t) = k_0 + k_1\lambda(t)$  [ $a_0, a_1, r_0, r_1, k_0$ , and  $k_1$  are constants and  $r(t) > 0$ ,  $K(t) > 0$ ],  $\mu > 0$ , admits a saddle–saddle connection if the phase portrait is admissible and  $\Delta m = N(S_1) - N(S_0) < 0$  or if the phase portrait is non-admissible with four fixed points and  $\Delta m > 0$ . We give the proof of this theorem in Appendix C.

We prove this by comparing the relative positions of the stable and unstable manifolds of  $S_1$  and  $S_0$ , respectively, when  $\mu$  is small and when  $\mu$  is large. We will prove that these manifolds intersect for some  $\mu$  and, thus, establish a saddle–saddle connection.

We state and prove three lemmata (in Appendix B) to help establish the theorem, which we then employ to identify tipping points in the growth of atmospheric carbon dioxide emissions from fossil fuel.

#### Non-admissible phase portraits with a saddle–saddle connection:

An example of such a portrait is Fig. 3(e). When we analyze the data of atmospheric carbon dioxide emissions from fossil fuels, we find that until now, there has been no transition where this kind of phase portrait has occurred. This might happen in the future when the carrying capacity  $K$  has an exponential growth (notice that  $\Delta m > 0$  implies that the unstable root of the next period would be larger than the stable root of the previous period—this points to a large growth in  $K$  as compared to the other type of phase portrait). Since the CO<sub>2</sub> growth curve is now approaching an exponential growth trend, we expect to see a non-admissible phase portrait in the future.

## III. RESULTS

### A. Critical value of $\mu$

$\mu_c$  is defined to be the critical value of  $\mu$  such that if  $\mu < \mu_c$ , a growth from one stable state to the next one does not occur. In the system, this means that trajectories starting out from  $S_0$  (the previous stable state) will not grow toward  $S_i$  (the next stable state) or  $S_1$ .

When  $\mu_c$  is attained, there is a saddle–saddle connection [see Fig. 3(f)].

We use a linear approximation of the saddle–saddle connection as in Ref. 13 to calculate  $\mu_c$ . The calculation is described in Appendix D. As the connection may not, in fact, be a straight line, we take the average of the estimate  $\mu_0$  at  $S_0$  and  $\mu_1$  at  $S_1$  to give an estimate of  $\mu_c$ ,

$$\mu_c = \frac{\mu_0 + \mu_1}{2} \quad (6)$$

[see Eq. (D5) in Appendix D].  $\mu$  is calculated from the data using Algorithm 2 (see Appendix E).

If we approximate the ramp part of  $\lambda$  by a line, we get the following relation:

$$\mu \approx \frac{4}{\Delta t}, \tag{7}$$

where  $\Delta t$  is the time taken for the ramp growth. If  $\mu > 4$ ,  $\Delta t < 1$ , so to actually find accurate values of  $\mu$  from the data, we should use monthly data (if given data are yearly), i.e., we need more resolution to measure  $\mu$  accurately if it is greater than 4.

### B. Asymptotic analysis

We observe in our system that rate-induced tipping is necessary for growth to the next stable state, but it is not sufficient. A sufficient condition is that the initial conditions must be within the basin of attraction. In our system under suitable conditions, the basin is approximately a rectangular region with sides  $\lambda = \pm 1$  and the bottom side given by the stable manifold of  $S_1$ . The rectangle is unbounded on top. Fortunately, for our system, the boundary of the basin can be approximated roughly by a line, and as  $\mu$  increases, the approximation is better. We denote the basin boundary given by the stable manifold of  $S_1$  by  $\psi_{stable}$ . Since it is not easy to calculate, we will derive a simpler condition to prevent growth even when rate-induced tipping has occurred.

Consider an admissible phase portrait and  $\Delta m < 0$  with  $\mu$  large [Fig. 4(a)].

Observe that for large  $\mu$  and  $N < m_1$ , the growth does not occur. This is because the stable manifold, i.e., the boundary of the basin, tends to the line  $N = m_1$  as  $\mu$  increases. Furthermore, the continuous dependence of  $\psi_{stable}$  on  $\mu$  ensures that the basin boundary is always above the line  $N = m_1$ .

More precisely, note that given any  $\epsilon > 0$ , we can choose  $\mu$  large enough such that  $|dN/d\lambda| < \epsilon$  in any closed set, which does not contain the lines  $\lambda = 0$  or  $\lambda = 1$  (as on these lines  $d\lambda/dt = 0$  and since  $d\lambda/dt$  is a function of  $\mu$ , while  $dN/dt$  is not and in any closed set maxima and minima are achieved). This line of reasoning shows that for a phase portrait, if  $\mu$  is large enough, the slopes  $|dN/d\lambda|$  are almost zero. The trajectories will then be approximately lines (except near  $\lambda = 0$  and  $\lambda = 1$ ), which give the observation above (since the stable manifold of  $S_1$  is approximately a line, i.e.,  $\psi_{stable}(\lambda) \approx m_1$ ).

The above observations allow us to define an easily calculable and measurable quantity  $N_{transition}$  that helps in choosing such an initial point, which would prevent growth.

We define  $N_{transition}$  to be the value of  $N$ , where  $\lambda = 0.5$  in the trajectory of growth (i.e., midway between the change in the parameters). From the observation above, we know that as  $\mu \rightarrow \infty$ , the approximation of  $\psi_{stable}(\lambda)$  as  $m_1$  gets better, and therefore, in the limit,  $\psi_{stable}(\lambda) = m_1$  (except at  $\lambda = 0$ ). Thus, if  $N_{transition} < m_1$ , no growth toward the next stable state occurs (if  $N_{transition} \geq m_1$  growth may occur depending on  $\mu$ ). See Fig. 4(b) for an illustration of  $N_{transition}$ . This gives us another condition, which is a measurable quantity.

Note that to prevent tipping, one must have  $\mu < \mu_c$ , and if this limit is exceeded, the only way to prevent growth to the next stable state is to prevent the growth of  $N$ , for which one must have  $N_{transition} < m_1$ .

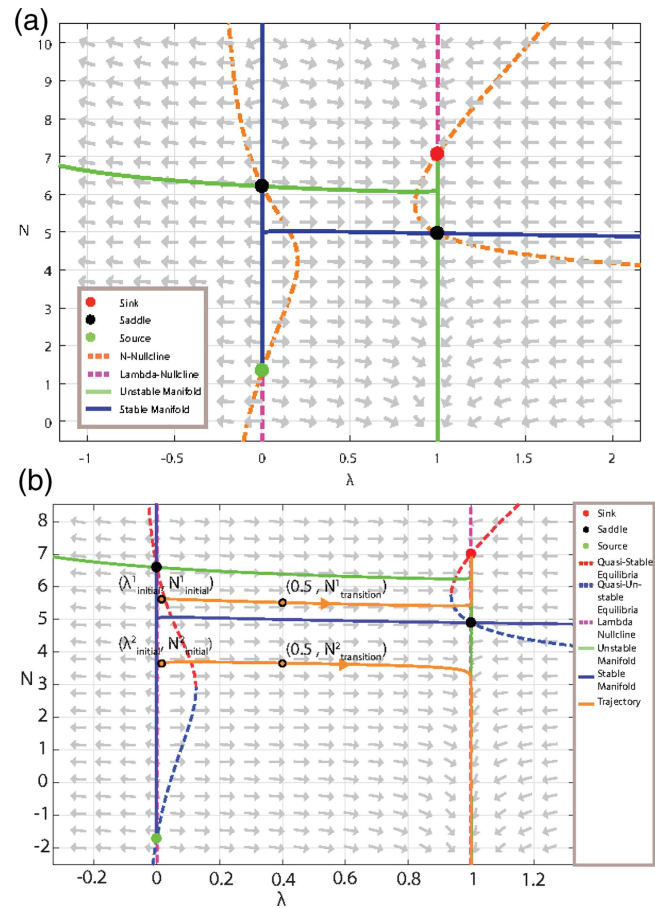


**FIG. 4.** (a) Admissible phase portrait,  $\mu$  large; (b) illustration of  $N_{transition}$ . Trajectories (in orange) are shown for two different initial conditions. Those starting from  $(\lambda^1_{initial}, N^1_{initial})$  grow toward the next stable state, while points starting from  $(\lambda^2_{initial}, N^2_{initial})$  fail to grow to the next stable state even though tipping has occurred.

Note that there is no  $N_{transition}$  for the non-admissible case since  $\Delta m > 0$ . Thus, in this case, only tipping can prevent growth.

In both admissible and non-admissible phase portraits, tipping happens if  $\mu > \mu_c$  (i.e., failure to follow the quasi-stable attractor). However, in the case of an admissible phase portrait, no tipping implies the failure to grow to the next stable state; i.e., the system is “predisposed” to not move toward the next stable state. Here, tipping causes growth to the next stable state (unless  $N_{transition} < m_1$ ). However, in the case of a non-admissible phase portrait, since there is an  $S_0$ - $S_1$  connection, without tipping, the system would grow from  $S_0$  to  $S_1$ ; i.e., this type of system is “predisposed” to grow unless tipping happens.

However, as we will see in Secs. III A–III F and Appendix A–G, when we apply the system to  $CO_2$  emissions data, the non-admissible portrait does not show up. It might only be useful when the growth of a system is uncontrolled and exponential.



**TABLE I.** Top: Table of parameters of the model [in Eqs. (1a) and (1b)]. Bottom: Comparison of predicted and fitted parameters for known transition periods using Eqs. (1a) and (1b).

Transitions period	$r$	$K$	$A_0$	$T_{\max}$
1850–1943	0.038	1.800	0.002	1920
1944–1953	3.014	3.181	−2.302	1950
1954–1962	0.0511	2.604	0.084	1949
1963–1980	0.583	7.616	−0.911	1969
1981–1999	1.505	11.741	−4.302	1989
2000–2009	3.033	15.490	−11.436	2004
2010–2015	17.346	18.124	−78.305	2010
2016–2022	20.000	20.200	−100.695	2019
2023–2029	39.400	22.860	−224.866	2025

Parameters	From data (fitted)			Predicted			
	$r$	$K$	$A_0$	$r$	$K$	$A_0$	$T_{\max}$
Period							
2000–2009	3.033	15.490	−11.436	3	15	−11.025	2005
2010–2015	17.346	18.124	−78.305	16	18.5	−73.7	2012

### C. Application to CO<sub>2</sub> data

The methods developed above are applied now to the *global carbon budget* data in Ref. 5 plotted in Fig. 1 (green squares).

In this figure, we have already marked the years where transitions occur. This was obtained from the derivative data. The derivatives were fit to quadratic polynomials as explained in Algorithm 1 of Appendix A.

The parameters obtained from this fitting are shown in Table I. Figures 5(a)–5(c) depict the plots of the parameters as step functions. Using these parameters, we can recalculate  $N$  using the equation  $N = \frac{1}{2}(K + \sqrt{\beta \frac{K}{r}} \tanh(\frac{1}{2}\sqrt{\beta \frac{r}{K}}(t - T_{\max})))$  to find out the goodness of fit. The result is displayed in Fig. 1 (green squares).

### D. Predictions

Now, we can use the data to predict two future transition periods using Algorithm 3. Parameters of the resulting transition periods are shown in red of Table I. These are plotted in Fig. 5(d) [see also Figs. 8(e) and 8(f)–8(h) in Appendix F].

Thus, the next transition may occur in early 2022 and is expected to be the transition to the next stable state unless  $\mu_{2022} < \mu_c = 0.802$  (calculated below). We can approximate  $N_{\text{transition}}$  for this period by just taking the predicted value of  $N$  at the transition point, i.e.,  $N(2022)$ . It comes out to be  $N_{\text{transition}} = 10.62$ .

We can use Algorithm 3 to predict known periods to check how good the method of prediction is. We will do it for the last two periods. The predicted data are displayed in Table I.

In Fig. 5(e), we plot our hindcast predictions of *known periods*, along with the known data.

We can also calculate  $\mu_c$  for each transition [using Eq. (D5)] and also the corresponding  $\mu$  from the data (using Algorithm 2 in Appendix E). The results are shown in Table II. The transition points obtained, thus, can be identified with climate change.

The phase portrait for the transition in 1980 is shown in Fig. 6(a). Those for all other transition years are displayed in Figs. 6(d)–6(h). As an illustration, Fig. 6(a) shows how the 1980 transition would look like for  $\mu < \mu_c$  [Fig. 6(b)] and for  $\mu > \mu_c$  [Fig. 6(c)].

Regime shifts in the Earth's climate occur as a consequence of changes in the physical environment—the atmosphere, land surfaces, oceans, and cryosphere and complex interactions between them.<sup>9,10</sup> Such shifts get manifested as visible changes in the climate-sensitive biosphere, for example, as changes in flowering times of plants, in population densities of various species, changes in migratory times and patterns of birds, and changes in the dynamics of various ecosystems over many years.

Several such changes in the biological realm signaling climatic regime shifts have been observed and documented. It is interesting to note that many of the transition years we find from the CO<sub>2</sub> data (1943, 1953, 1980, 1999, 2009, and 2015) lie roughly near the transition years 1947, 1977, 1999, 2007, and 2014 for the Pacific Decadal Oscillations (PDOs)<sup>14</sup>—oscillations between the warm and cool phases in the surface waters of the Pacific ocean. The PDO itself is understood to arise as a consequence of different physical processes, including interactions between the atmosphere and oceans.<sup>15</sup>

It was noted in Ref. 16 that decadal regime shifts in the populations of anchovies and sardines in the Pacific ocean occur in association with switches between warmer and cooler than average ocean temperatures. Considering the 1950–1976 and 1977–1999 regimes, they pointed out that such abrupt biological regime shifts should be driven by large-scale oceanic and atmospheric processes, including fluctuations of carbon dioxide in the atmosphere.

It has been shown that fish populations are sensitive to climate change indicators, such as the PDO and North Atlantic Ocean (NAO) indices.<sup>17</sup> Similarly, bird populations were shown to be synchronous with PDO and NAO linked sea surface temperature (SST) changes identified as climatic regime shifts in 1977 and 1989.<sup>18</sup> A regime shift delay in the onset of the Indian summer monsoon following the 1976/1977 Pacific SST regime shift has been reported in Ref. 19. Using data from the Arctic oscillation (AO) index, the Atlantic multidecadal oscillation (AMO) index, the NAO index, and regional sea level pressure (SLP) anomalies, regional area averaged monthly SST anomalies, and benthic macrofauna samples, it was shown in Ref. 20 that biological regime shifts occurred in 2000/2001 caused by a climatic regime shift.

The year 2000 has been shown to be a regime shift year in the decadal variation of the Indian Ocean SST caused by a regime shift in equatorial zonal surface wind patterns, which influence the Indian monsoon.<sup>21</sup>

The years 1956–1957, 1964–1965, 1988–1989, and 1998–1999 have been identified in Ref. 22 as significant regime shift years for marine fish landings globally, associating these with approximate shift years in the normalized atmospheric planetary wave amplitude index. Planetary wave activity is known to weaken under the influence of global warming from CO<sub>2</sub> forcing.<sup>23</sup>

The assessment of radiosonde atmospheric temperature measurement data at the Payerne Swiss aerological station for the period 1959–2011 in Ref. 24 shows warming in the troposphere and cooling in the stratosphere since the 1960s, with three clearly

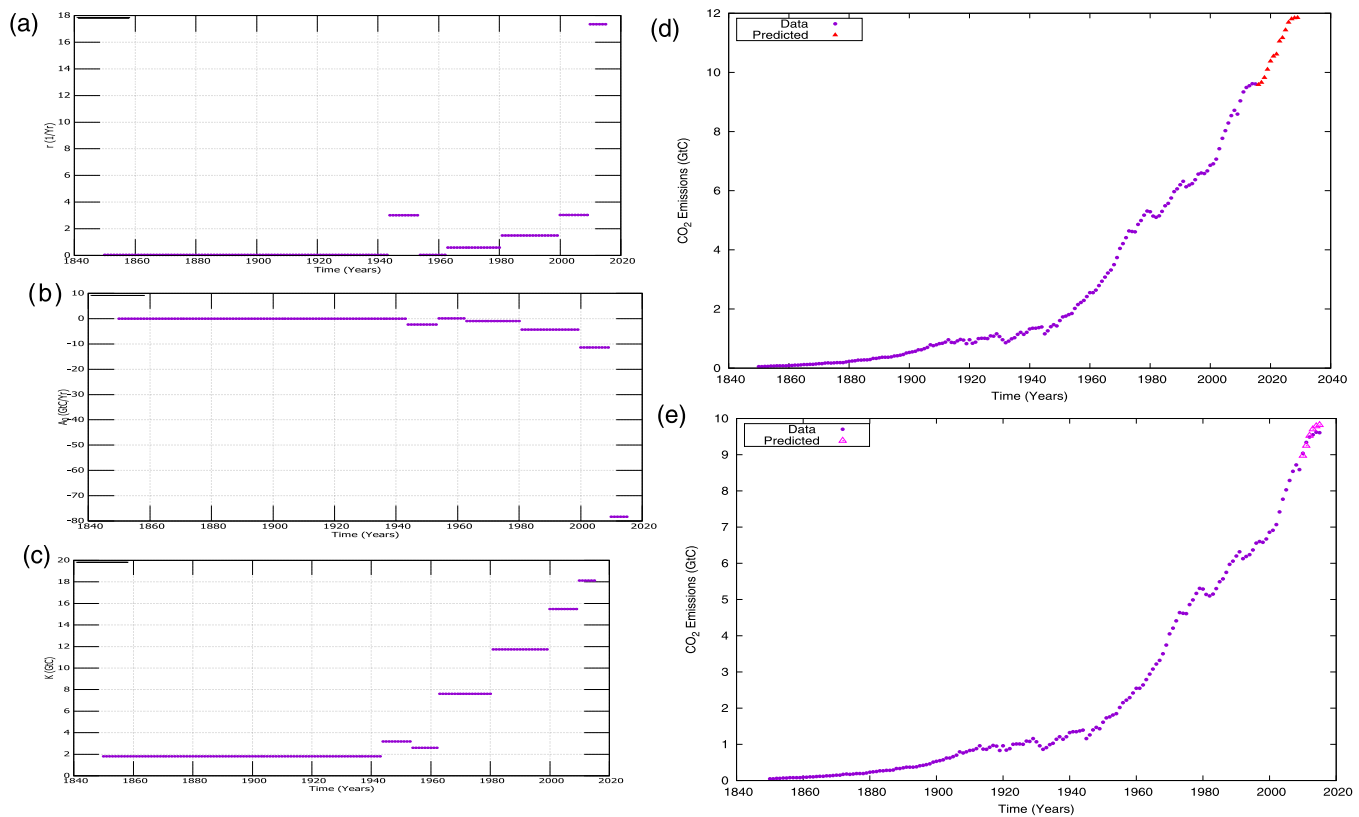


**FIG. 5.** Model predictions and growth curves. (a)  $r$  vs  $t$ , (b)  $A_0$  vs  $t$ , (c)  $K$  vs  $t$ , (d) predictions from the model for two future transition periods (2016–2022 and 2023–2029) shown as red triangles, and (e) hindcast prediction (magenta triangles) of atmospheric fossil-fuel  $\text{CO}_2$  emissions for known transition periods (2000–2009 and 2009–2015).

distinct trends, respectively, for the periods 1959–1980, 1980–2000, and 2001–2011. These point to a transition to different climatic regimes in the transition years 1980, 2000, and 2011. These years, which we identify as transition years in our model, are, therefore, in close agreement to those identified as possible climatic regime

shift years in the literature. Thus, the transition years (noted as such from our model) seem to have a clear impact on the climate as seen in both the ocean sink data as well as in the temperature anomaly data. The transition at 1943 could have been caused by the rapid industrialization of the World War II era.

**TABLE II.** Calculated values of  $\mu$ . Predicted values are shown in red.

Transition point	$\mu_1$	$\mu_0$	$\mu_c = \frac{\mu_0 + \mu_1}{2}$	$\mu_{calc} = \mu(\text{alg.2})$	$\mu_c$ (from phase portrait)	Mean % error at $\mu_{calc}$
1943	0.478	4.103	2.290	11.98	1.8	10.91
1953	2.281	-0.434	0.923	7.25	0.004 <sup>a</sup>	3.17
1962	-0.196	0.767	0.285	22	0.05 <sup>a</sup>	1.20
1980	0.429	1.222	0.826	5.78	0.77	1.34
1999	1.389	2.364	1.877	31	1.85	1.28
2009	14.665	20.052	17.358	64	17	0.44
2015	0.609	0.994	0.802	No data	...	...
2022	23.656	25.829	24.742	No data	...	...

<sup>a</sup>The saddle–saddle connection could not be computed precisely due to numerical limitations. The given  $\mu_{phase}$  is an approximation. The last column shows the mean percentage error  $L'$  at  $\mu_{calculated}$ .

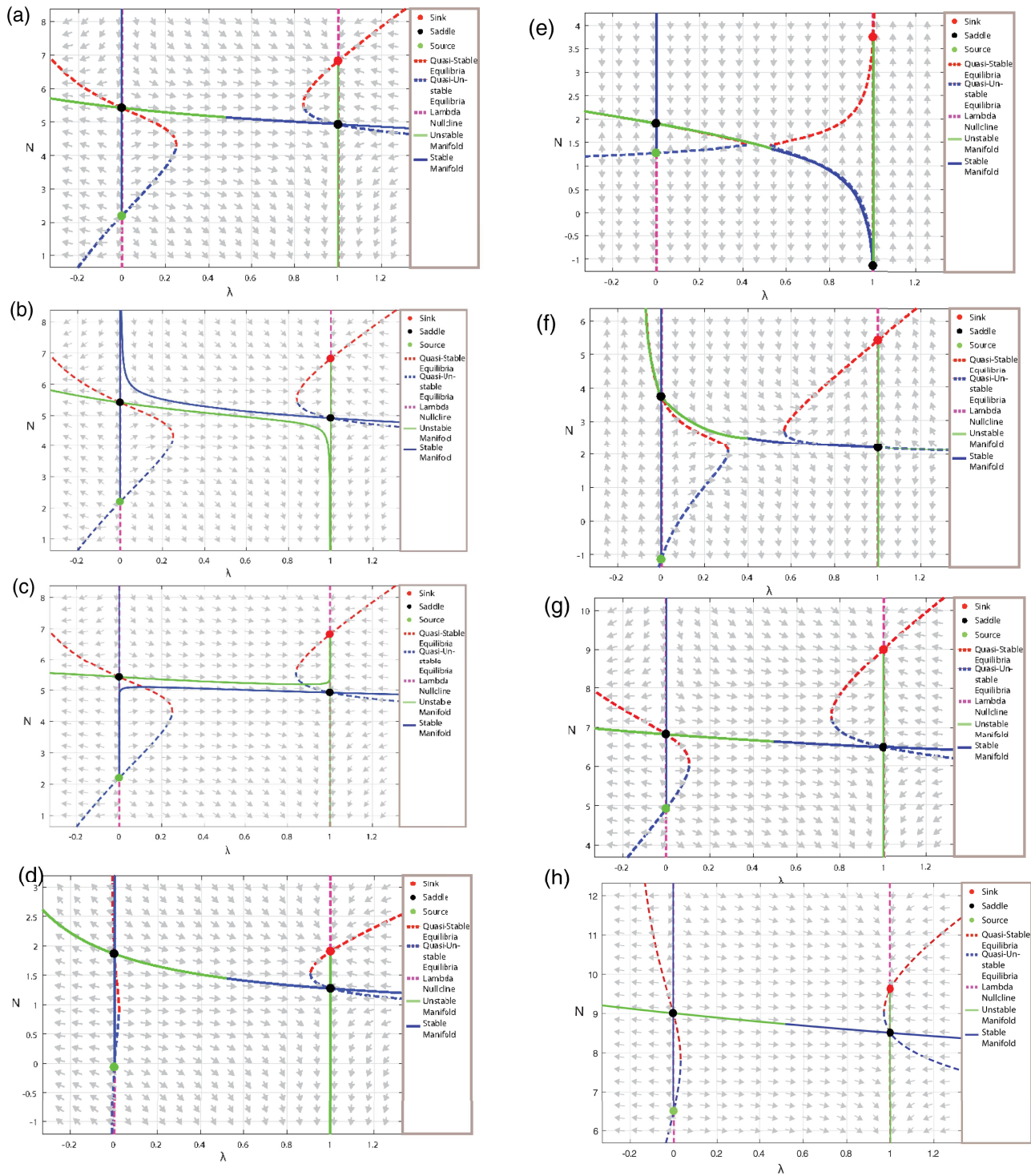


**FIG. 6.** Tipping/transition years predicted by the model: (a) transition of 1980,  $\mu_c = 0.77$  (from the phase portrait); (b) phase portrait for 1980 for  $\mu = 0.5$  ( $\mu < \mu_c$ ); and (c) phase portrait for 1980 for  $\mu = 6.8$  ( $\mu > \mu_c$ ). Transition of (d) 1943, (e) 1953, (f) 1962, (g) 1999, and (h) 2009.

Interestingly, the algorithm proposed in Ref. 25 detected regime shifts in the winter PDO as occurring in 1946, 1977, and 2003 and in the summer and annual PDO as occurring in 1943, 1976, and 1998.<sup>25,26</sup> While the years 1999–2000, 2000–2001, 2008–2009, 2011–2012, and 2010 have been identified in the literature as strong La Niña years, the years 1998–1999 and 2016–2017 have been identified as very strong El Niño years.

### E. Temperature anomaly and CO<sub>2</sub> emissions

From the temperature anomaly graph and the CO<sub>2</sub> emissions graph [Fig. 7(a)], we can see that the transition points we identified are indeed important. Since temperature is a major part of climate, we can argue that climate will be affected by the change of CO<sub>2</sub> emissions. From the predictions we obtained in Secs. III A–III D and since  $\mu \approx \frac{4}{\Delta t}$ , transitions in CO<sub>2</sub> growth and correspondingly climate transitions will speed up as  $\mu$  increases. To prevent the transition at the start of 2022, we must have  $\mu_{2022} < \mu_c = 0.80201$ . However, this parameter cannot change directly, and since  $\mu_{2009} = 64$ , it is likely that  $\mu_c$  will be exceeded in 2022. Even so, we still have  $N_{transition}(2022) = 10.62$ , and so if we can have global CO<sub>2</sub> emissions less than 10.62 GtC before early 2022/at the start of 2022, we should be able to avoid tipping.

### F. Ocean sink and A<sub>0</sub>

$A_0$  is the rate of CO<sub>2</sub> emission when  $N = 0$ . As shown in Fig. 7(b), it correlates with the ocean sink of CO<sub>2</sub>, which is to be expected since the oceans play an important role in the global carbon cycle.<sup>27,28</sup>

Negative  $A_0$  values physically mean that some amount of CO<sub>2</sub> in the atmosphere is necessary for stable growth. If  $N_{CO_2}$  is less than this amount ( $N_{unstable\ root}$ ), then  $N \rightarrow 0$ .  $A_0$  positive means that CO<sub>2</sub> is coming into the atmosphere from some source and is never zero.

A negative value for  $A_0$  means that CO<sub>2</sub> has a minimum positive concentration in the atmosphere. Any concentration less than this value leads to removal of CO<sub>2</sub> from the atmosphere. This is because if  $A_0 < 0$ , then as  $A_0$  is the rate at  $N = 0$ , both roots of the  $dN/dt$  equation must be positive. The above observation then follows directly from the fact that the unstable root has a positive value.

In the case where  $A_0 > 0$ , CO<sub>2</sub> is pumped into the atmosphere even if the original concentration was zero. This means that there will always be CO<sub>2</sub> in the atmosphere, and there is not a minimum concentration as in the previous case. The ocean can be both a CO<sub>2</sub> sink and source depending on the condition of the ambient atmosphere and temperature. Thus,  $A_0$  could be a measure of the sink/source state of the ocean.

It may be noted that for the growth period of 1954–1962 [ $\lambda = 0$  line in Fig. 6(f)], the smaller root is negative. This is because  $A_0$  is positive in this period. Since in between the roots, all flow directions must point toward the larger root, and since  $dN/dt = A_0$  when  $N = 0$ , the smaller root has to be negative since only then would the flow directions at  $N = 0$  point toward the larger root, i.e., upward. Physically, only the larger roots in a period are important since growth is from one stable state to the next. Negative valued  $N$  would imply the sinks (ocean, land, etc.) are absorbing more carbon than is

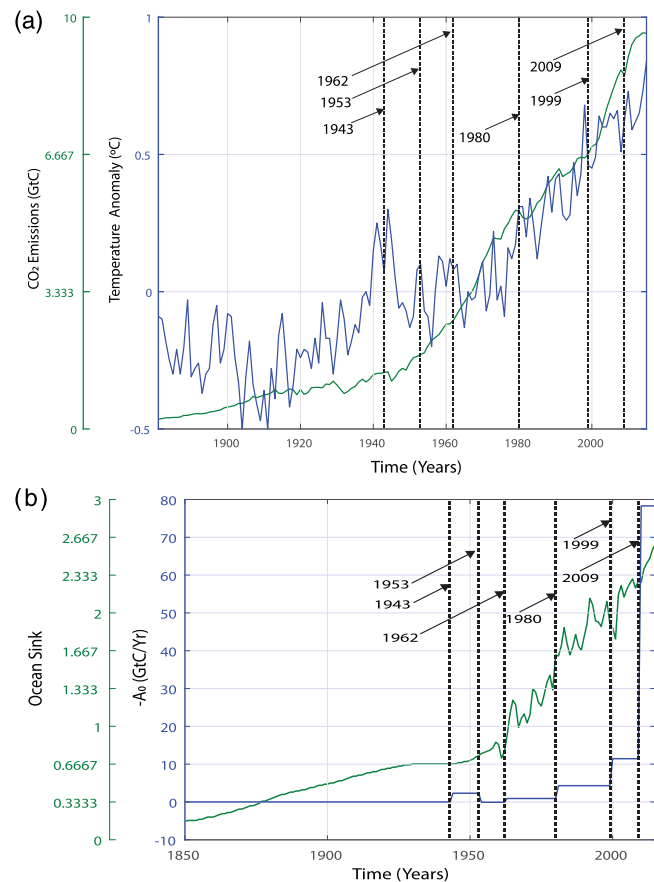


FIG. 7. (a) Plot of the temperature anomaly and CO<sub>2</sub> emissions. (b) CO<sub>2</sub> ocean sink and  $-A_0$ .

added in the atmosphere. We recall here that all stable roots are positive. In our case here, where one unstable root is negative, we can say that any amount of CO<sub>2</sub> in the atmosphere would sustain itself and in fact grow. This is because since in this case,  $A_0 > 0$  even if  $N = 0$ , i.e., no CO<sub>2</sub> in the atmosphere, the ocean would input some CO<sub>2</sub> causing growth. Thus, a negative valued unstable fixed point has a physical interpretation.

## IV. CONCLUSIONS

It is well established that there is a direct relation between CO<sub>2</sub> in the atmosphere and temperature. The main reason for the increase of CO<sub>2</sub> in the atmosphere causing a temperature increase and consequently bringing about a rapid climate change is the consumption of fossil fuels. We show that our model has two distinct tipping mechanisms driven by measurable parameters.

Our model and methods can help to identify the tipping points in the growth of CO<sub>2</sub> emissions and consequently in climatic systems from meaningful quantities ( $\mu_c$ ,  $N_{transition}$ ) that help in prescribing the limits, which should not be crossed to prevent a climate change.

Our method can also, in general, be applied to any growth curve to identify rate-induced tipping.

With the presently available data, we predict that the climatic system would tip over to a new stable state in early 2022. We find that if global CO<sub>2</sub> emissions can be limited to less than 10.62 GtC at the start of 2022, tipping can be avoided.

If the growth of a trajectory fails, it tends to  $-\infty$ ; however, this may not actually happen in the real system. In the real system, this could be interpreted as either “stalling” of growth or even perhaps loss of CO<sub>2</sub> concentration; other mechanisms may kick in at this point and the CO<sub>2</sub> concentration may stabilize. However, this has so far not happened in our data. In our data, CO<sub>2</sub> has grown continuously. It is not known at this point whether the model can handle negative growth rates since this violates the positivity condition. This could be a future avenue for further study.

We note that real-world processes are stochastic in nature, and therefore, the actual tipping processes would involve stochastic elements. Perturbations leading to planetary state shifts could lead to completely changed and entirely different dynamical scenarios for the system, including the possibility of transient chaos. We do not consider such perturbations in our system in this work.

Our model is a conceptual one, aimed to be of use as a tool for detecting tipping points in data already extant, to allow calculation of tipping rates and to predict future ones, given enough data. We have not considered a stochastic model because we want at this level of abstraction a model that allows one to make such calculations easily. Our model appears to work well as it is. Investigating the more complex situations with stochastic elements would be outlook for future work.

## ACKNOWLEDGMENTS

J.B. and E.M.S. were supported by the research grant SPG/2021/001410 from the Science and Engineering Research Board, Department of Science and Technology, Government of India.

## AUTHOR DECLARATIONS

### Conflict of Interest

The authors have no conflicts to disclose.

## Author Contributions

**Eros M. Sunny:** Data curation (lead); Formal analysis (equal); Investigation (equal); Methodology (equal); Validation (equal); Visualization (lead); Writing – original draft (equal); Writing – review & editing (equal). **Janaki Balakrishnan:** Conceptualization (lead); Formal analysis (equal); Funding acquisition (lead); Investigation (equal); Methodology (equal); Project administration (lead); Supervision (lead); Validation (equal); Visualization (supporting); Writing – original draft (equal); Writing – review & editing (equal). **Jürgen Kurths:** Formal analysis (equal); Investigation (equal); Methodology (equal); Validation (equal); Visualization (supporting); Writing – original draft (equal); Writing – review & editing (equal).

## DATA AVAILABILITY

The data that support the findings of this study are openly available in the Global Carbon Project at <https://doi.org/10.5194/essd-2021-386>, Ref. 5.

## APPENDIX A: FITTING AND CALCULATION OF PARAMETERS

The logistic equation is easy to fit when we are dealing with a single phase of growth.

From the assumption that the parameters are step functions of time, we can infer that on an interval of time where the parameters are constant, Eq. (1a) has the solution,

$$N = \frac{1}{2} \left( K + \sqrt{\frac{\beta K}{r}} \tanh \left( \frac{1}{2} \sqrt{\frac{\beta r}{K}} (t - T_{\max}) \right) \right), \quad (\text{A1})$$

where  $\beta = Kr + 4A_0$  and  $T_{\max}$  is the value of  $t$  in one period of growth at which  $\frac{dN}{dt}$  attains its maximum.

However, in most real systems, such as the global CO<sub>2</sub> fossil-fuel emissions data, one can expect multiple phases of growth. In this case, if  $N$  is the data, we calculate  $dN/dt$ , i.e., the derivatives, and plot it against  $N$ . We fit the data to Eqs. (1a) and (1b) following Algorithm 1 (described below). We expect (if the growth was approximately logistic) for each period of growth a quadratic peak (since  $\frac{dN}{dt} = A_0 + rN - \frac{r}{K}N^2$ ). We can fit each such peak separately [see Figs. 8(a) and 8(b)]. Once we have fitted each peak, we use the parameters obtained  $r$ ,  $K$ ,  $A_0$  and put them into the solution in (A1).  $T_{\max}$  is the constant of integration, which we have to choose such that the fit is the best. Thus, we can recalculate  $N$  allowing us to compare the goodness of fit.

Once we have the parameters for all phases of growth, we can put these values together to obtain step functions for each parameter. Further analysis is done on the transitions of these step functions (transitions of all parameter step functions occur simultaneously by the nature of the fit).

We can also extrapolate the data curve further and predict the future growth curve. We do this using Algorithm 3 (discussed below).

We shall start with the algorithm for fitting the data.

### Algorithm 1: Fitting the data

1. Let  $D = (t, N)$  be the dataset with  $t = \text{time}$  and  $N = \text{data}$ . Calculate  $dN/dt$  for various levels of smoothing. *Smoothing:* To calculate the derivatives, we first smooth the CO<sub>2</sub> data using a cubic spline and then calculate derivatives from this cubic spline. The parameter  $\phi \in (0, 1]$  determines to which extent the data are smoothed. A larger value of  $\phi$  denotes higher smoothing. In our study, we have used  $\phi = 0.2$ . We use the function `smooth.spline` (which is standard in R) to fit a cubic spline to CO<sub>2</sub> data (denoted  $\{t_i, N_i\}_i$ ). The cubic spline estimate  $f$  minimizes

$$L = \sum_i (N_i - f(t_i))^2 + \lambda \int \frac{d^2 f}{dt^2} dt$$

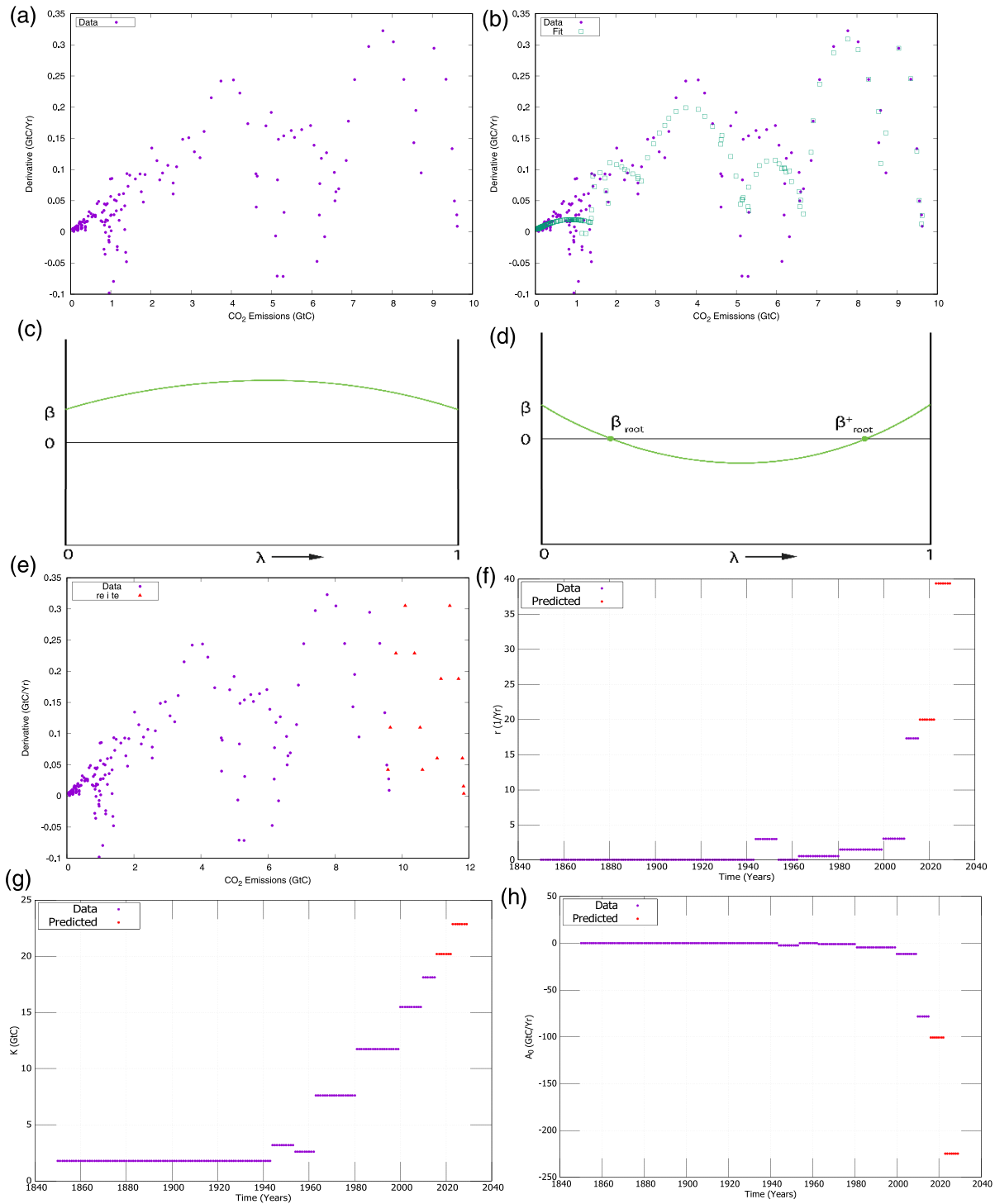


**FIG. 8.** Fitting of growth curves and parameter extraction: (a) Derivative  $dN/dt$  vs  $N$  (CO<sub>2</sub> emissions). (b) Derivative  $dN/dt$  vs  $N$  (CO<sub>2</sub> emissions) along with the fit of derivatives (green squares). (c)  $\beta$  has no roots in the domain. (d)  $\beta$  has roots in the domain. (e)  $dN/dt$  vs  $N$  with predictions shown as red triangles. (f)  $r$  vs  $t$  with predictions shown in red. (g)  $K$  vs  $t$  with predictions shown in red. (h)  $A_0$  vs  $t$  with predictions shown in red.

over the class of twice differentiable functions. The parameter  $\phi$  controls  $\lambda$  by the equation  $\lambda = r \times 256^{3\phi-1}$ . Here,  $r = \text{tr}(X'WX)/\text{tr}(\Sigma)$ , where  $X, W$  and  $\Sigma$  are certain matrices. The code works by solving a linear system under the above minimization condition.

- After considering plots of  $dN/dt$  vs  $N$  for various levels of smoothing, pick out the quadratic peaks by partitioning  $D' = (t, N, dN/dt)$  such that in each sub-dataset, there is only one quadratic peak (after the choice of time points where the data are to be partitioned is decided, we use unsmoothed (or little smoothing) derivatives for further calculations) [see Figs. 8(a) and 8(b)].
- Fit each sub-dataset to the equation  $\frac{dN}{dt} = A_0 + rN - \frac{r}{K}N^2$ , where the parameters  $A_0, r, K$  are to be found.
- Repeat step 3 for all sub-datasets.

**APPENDIX B: THREE LEMMATA AND A THEOREM**

We do not consider cases with less than four fixed points as these quasi-stable equilibria might not exist for certain fixed points. For example, consider the case where there are three fixed points. This happens if two fixed points on  $\lambda = 0$  (or  $\lambda = 1$ ) have become equal. Then, no quasi-stable equilibria do exist for this fixed point for  $\lambda > 0$  as no roots of  $dN/dt = 0$  do exist after this point. Since the focus of our work is rate-induced tipping for which quasi-equilibria are necessary, we will not consider cases where the number of fixed points is less than 4.

The following three lemmata are useful in proving the theorem we have stated below, which gives conditions for admitting saddle–saddle connections, which define rate-induced tipping points.

Lemmata:

- Lemma 1: There are at most four fixed points.*  
We shall solve Eqs. (1a) and (1b) for fixed points.  $d\lambda/dt = 0$  and  $dN/dt = 0$  give  $\lambda = 0$  and  $\lambda = 1$ . Putting these values in  $dN/dt = 0$  gives

$$a_0 + r_0N - \frac{r_0}{k_0}N^2 = 0, \tag{B1}$$

$$a_0 + a_1 + (r_0 + r_1)N - \frac{r_0 + r_1}{k_0 + k_1}N^2 = 0,$$

which gives at most four solutions.

- Lemma 2: If there are four fixed points, then  $N(S_0) > N(Se)$  and  $N(Si) > N(S_1)$ .*

This means that on the  $\lambda = 0$  line, always,  $Se$  is below  $S_0$ , and on the other line,  $S_1$  is below  $Si$ . This can be proved easily. The Jacobian  $J(\lambda, N)$  is

$$\begin{pmatrix} \mu(1 - 2\lambda) & 0 \\ \eta(\lambda, N) & \omega(\lambda, N) \end{pmatrix}, \tag{B2}$$

with  $\eta(\lambda, N) = a_1 + r_1N - \frac{r_1(k_0+k_1\lambda)-k_1(r_0+r_1\lambda)}{(k_0+k_1\lambda)^2}N^2$  and  $\omega(\lambda, N) = (r_0 + r_1\lambda)(1 - \frac{2N}{(k_0+k_1\lambda)})$ . The two fixed points on  $\lambda = 0$  are

$$N = \frac{k_0r_0 \pm k_0\sqrt{r_0^2 + 4\frac{r_0a_0}{k_0}}}{2r_0} = \frac{k_0}{2} \pm \frac{k_0}{2r_0}\Omega, \tag{B3}$$

where  $\Omega = \sqrt{r_0^2 + 4\frac{r_0a_0}{k_0}} > 0$ . Let  $N_1 = \frac{k_0}{2} + \frac{k_0}{2r_0}\Omega$  and  $N_2 = \frac{k_0}{2} - \frac{k_0}{2r_0}\Omega$ . Clearly,  $N_1 > N_2$  [since  $r(t) > 0, K(t) > 0$ ]. The eigenvalues of the Jacobian on  $\lambda = 0$  are  $\mu$  and  $r_0(1 - \frac{2N}{k_0})$ . Then,

$$r_0\left(1 - \frac{2N}{k_0}\right) = r_0\left(1 - \left(1 \pm \frac{\Omega}{r_0}\right)\right) = \mp\Omega. \tag{B4}$$

Thus, for  $N_1$ , we have eigenvalues  $\mu > 0$  and  $-\Omega < 0$ , which means that the fixed point at  $(0, N_1)$  is a saddle, and similarly, for  $N_2$ ,  $\mu > 0$  and  $\Omega > 0$ , i.e., a source. Given  $N_1 > N_2$ , we have that  $Se$  is below  $S_0$ . We can proceed similarly for the  $\lambda = 1$  line and get that  $Si$  lies above  $S_1$ . We let  $m_0$

$$m_0 = \frac{k_0r_0 + k_0\sqrt{r_0^2 + 4\frac{r_0a_0}{k_0}}}{2r_0} = N(S_0) \text{ and } m_1 = N(S_1).$$

$$m_1 = \frac{(k_0+k_1)(r_0+r_1) - (k_0+k_1)\sqrt{(r_0+r_1)^2 + 4\frac{(r_0+r_1)(a_0+a_1)}{(k_0+k_1)}}}{2(r_0+r_1)}.$$

- Lemma 3: A phase portrait is admissible iff there is a  $S_0$ – $Se$  connection and no  $S_0$ – $Si$  connection.*

*Proof:* Consider the equation of the  $N$ -nullclines,

$$N(\lambda) = \frac{K(\lambda)r(\lambda) \pm K(\lambda)\sqrt{r^2(\lambda) + 4\frac{r(\lambda)A_0(\lambda)}{K(\lambda)}}}{2r(\lambda)}. \tag{B5}$$

The equation is quadratic [ $r(t) > 0, K(t) > 0$ ] for a given  $\lambda$ . So, at any  $\lambda$ , there are at most two points of the  $N$  nullcline. The nullcline does not exist if  $r^2(\lambda) + 4\frac{r(\lambda)A_0(\lambda)}{K(\lambda)} < 0 \iff \beta(\lambda) = K(\lambda)r(\lambda) + 4A_0(\lambda) < 0$  [see Figs. 8(c) and 8(d)]. Expanding this, we get the polynomial inequality

$$(k_0r_0 + 4a_0) + \lambda(k_0r_1 + k_1r_0 + 4a_1) + k_1r_1\lambda^2 < 0. \tag{B6}$$

Consider the polynomial  $P(\lambda) = (k_0r_0 + 4a_0) + \lambda(k_0r_1 + k_1r_0 + 4a_1) + k_1r_1\lambda^2$ . This polynomial encodes the behavior of the nullclines. It can be checked that  $P(0)$  and  $P(1)$  are both strictly positive. Then, in an interval around  $\lambda = 0$  and  $\lambda = 1$ , the polynomial is positive since it is continuous. If both roots of  $P(\lambda) = 0$  are different, then both either lie in  $\lambda \in [0, 1]$  or outside. This follows since if only one root lays in  $[0, 1]$ , then  $P(0)$  and  $P(1)$  would have opposite signs or one of them would be a zero, both of which are not acceptable (if one of them is a zero, then there would not be four fixed points). If the roots are outside (both roots are the same or different),  $P(\lambda) > 0$  for all  $\lambda \in [0, 1]$ . Thus, for every  $\lambda \in [0, 1]$ , there would be 2 points on the nullcline. This would imply an  $S_0$ – $Si$  connection and  $S_1$ – $Se$  connection [the other possibility is ruled out since both nullclines cannot cross ( $P(\lambda) > 0$ )]. If both roots (roots different) are in  $[0, 1]$ , then for some interval in  $[0, 1]$ ,  $P(\lambda) < 0$  and the nullclines do not exist. This implies an  $S_0$ – $Se$  and  $S_1$ – $Si$  connection. If there is only one single root and it lies in  $[0, 1]$ , then there are simultaneously all four connections:  $S_1$ – $Si$ ,  $S_1$ – $Se$ ,  $S_0$ – $Se$ , and  $S_0$ – $S_1$ . This would not be an admissible portrait. From the above line of reasoning, it is clear that  $S_0$ – $Se$  connection and no  $S_0$ – $Si$  connection  $\iff S_1$ – $Si$  connection and no  $S_1$ – $Se$  connection  $\iff$  admissible. Additionally, a non-admissible phase portrait with four fixed points has all four connections simultaneously

or  $S_1$ – $S_e$  and  $S_0$ – $S_i$  connections. The above discussion also gives the following condition for an admissible phase portrait:

$$\beta_{roots}^{\pm} = \frac{-(k_0 r_1 + k_1 r_0 + 4a_1)}{2k_1 r_1} \pm \frac{\sqrt{(k_0 r_1 + k_1 r_0 + 4a_1)^2 - 4k_1 r_1(k_0 r_0 + 4a_0)}}{2k_1 r_1} \in (0, 1). \tag{B7}$$

This also implies that  $k_1 r_1 > 0$ ; i.e,  $K$  and  $r$  must have the same change of sign.

**APPENDIX C: PROOF OF THE THEOREM**

We wish to show the existence of a saddle–saddle connection at some  $\mu$ . We will prove the statement of the theorem by observing that the stable manifold of  $S_1$  is close to the N-nullcline for small  $\mu$  and will move “downward” as  $\mu$  increases. Similarly, the unstable manifold of  $S_0$  is close to the N-nullcline for small  $\mu$  and will move “upward” with increasing  $\mu$ . For very large  $\mu$ , they must eventually “flatten out” and be approximable by the lines  $N = m_1$  and  $N = m_0$ , respectively. Since  $\Delta m < 0$ , this means that the manifolds should have intersected somewhere in between.

Let  $N = \psi_{unstable}(\lambda)$  and  $N = \psi_{stable}(\lambda)$  be the equations of the stable and unstable manifolds of  $S_1$  and  $S_0$ , respectively.

Let  $(\lambda, \psi_{unstable}(\lambda)) \in Unstable(S_0)$  ( $\lambda$  is fixed), we apply the mean value theorem to get

$$\frac{\psi_{unstable}(\lambda) - m_0}{\lambda - 0} = \frac{dN}{d\lambda}(\lambda_0, \psi_{unstable}(\lambda_0)),$$

where  $(\lambda_0, \psi_{unstable}(\lambda_0))$  is some point in between  $(0, m_0)$  and  $(\lambda, \psi_{unstable}(\lambda))$  on  $Unstable(S_0)$ . Similarly, construct the relation for  $Stable(S_1)$  with the point  $(\lambda, \psi_{stable}(\lambda))$  (the same  $\lambda$ )

$$\frac{\psi_{stable}(\lambda) - m_1}{\lambda - 1} = \frac{dN}{d\lambda}(\lambda_1, \psi_{stable}(\lambda_1)),$$

where  $(\lambda_1, \psi_{stable}(\lambda_1))$  is some point in between  $(1, m_1)$  and  $(\lambda, \psi_{stable}(\lambda))$  on  $Stable(S_1)$ . Then,

$$\begin{aligned} &\psi_{stable}(\lambda) - \psi_{unstable}(\lambda) - \Delta m \\ &= (\lambda - 1) \frac{dN}{d\lambda}(\lambda_1, \psi_{stable}(\lambda_1)) - \lambda \frac{dN}{d\lambda}(\lambda_0, \psi_{unstable}(\lambda_0)) \\ &= -(\lambda) \frac{dN}{d\lambda}(\lambda_0, \psi_{unstable}(\lambda_0)) + (1 - \lambda) \frac{dN}{d\lambda}(\lambda_1, \psi_{stable}(\lambda_1)) \\ &= \Delta D(\lambda, \mu) \\ &\psi_{stable}(\lambda, \mu) - \psi_{unstable}(\lambda, \mu) = \Delta D(\lambda, \mu) + \Delta m. \end{aligned}$$

The quantity  $\psi_{stable}(\lambda)$  is always defined and finite for  $\lambda \in (0, 1)$  since the stable manifold must connect to a fixed point or be asymptotic to  $\lambda = 1$ . Similarly,  $\psi_{unstable}(\lambda)$  is also finite and well defined for  $\lambda \in (0, 1)$ . Therefore, the difference  $\psi_{stable}(\lambda) - \psi_{unstable}(\lambda)$  makes sense for  $\lambda \in (0, 1)$ . Also, in the last line, we made the implicit dependence on  $\mu$  explicit. Since  $\psi_{stable}$  and  $\psi_{unstable}$  are trajectories, they are solutions of the system and, hence, are continuous in  $\mu$ . The LHS is continuous in  $\mu$ ; therefore, the RHS, in particular,  $\Delta D(\lambda, \mu)$ ,

must be continuous in  $\mu$  for  $\mu > 0$ . Note that if  $\Delta D(\lambda, \mu) = -\Delta m$  for a fixed  $\lambda$ , we have  $\psi_{stable}(\lambda, \mu) - \psi_{unstable}(\lambda, \mu) = 0$ , and if there is one point of intersection between the unstable and stable manifolds, then they intersect at all points. Thus, we have a saddle–saddle connection.

**1. Admissible phase portrait**

There exists an interval  $I \subset [0, 1]$  where no nullclines exist and  $\frac{dN}{d\lambda} < 0$  for all such  $\lambda \in I$  and any  $N$ . Pick some  $\lambda_a \in I$  and observe that  $\frac{dN}{d\lambda}(\lambda, \psi_{unstable}(\lambda)) < 0$  for all  $0 < \lambda < \lambda_a$  since if it were positive, it would mean that  $\psi_{unstable}$  passes into the region enclosed nullcline. However,  $\psi_{unstable}$  starts above the nullcline—at  $(0, m_0)$ —and since  $\frac{dN}{d\lambda}(\lambda, N) > 0$  within the region inside the nullcline,  $\psi_{unstable}$  cannot pass into it. A similar line of reasoning gives  $\frac{dN}{d\lambda}(\lambda, \psi_{stable}(\lambda)) < 0$  for all  $\lambda_a < \lambda < 1$ . Thus,  $\Delta D(\lambda_a) > 0$  since  $\lambda_0 \in (0, \lambda_a)$  and  $\lambda_1 \in (\lambda_a, 1)$ . We also note that when we let  $\mu \rightarrow \infty$ ,  $\Delta D(\lambda, \mu) \rightarrow 0$  since  $\frac{dN}{d\lambda} \rightarrow 0$  for all  $\lambda$  and  $N$ . Suppose  $\lambda_b \in I$  and  $\psi_{unstable}(\lambda_b, \mu)$ ,  $\psi_{stable}(\lambda_b, \mu)$  are the intersection of the unstable and stable manifolds with  $\lambda = \lambda_b$ . Then, as  $\mu \rightarrow 0$ ,  $\frac{dN}{d\lambda} \rightarrow -\infty$  on  $\lambda = \lambda_b$ , and since there are no nullclines intersecting with  $\lambda = \lambda_a$ ,  $\frac{dN}{d\lambda}(\lambda_b, \mu) < 0$  for all  $\mu$  and the difference  $\psi_{stable}(\lambda_b, \mu) - \psi_{unstable}(\lambda_b, \mu)$  increases. Thus,  $\Delta D(\lambda_b, \mu) \rightarrow \infty$ , and therefore, if  $\Delta m < 0$ , we can adjust  $\mu$  and, thus, obtain some  $\mu_c$  and a fixed  $\lambda$  where  $\Delta D(\lambda, \mu) = -\Delta m$ .

**2. Non-admissible phase portrait**

When  $\mu \rightarrow 0$ , the stable and unstable manifolds closely follow the nullclines, and therefore,  $\psi_{stable}(\lambda, \mu) - \psi_{unstable}(\lambda, \mu) < 0$ . However, when  $\mu \rightarrow \infty$ , we have  $\Delta D(\lambda, \mu) \rightarrow 0$ , and therefore  $\psi_{stable}(\lambda, \mu) - \psi_{unstable}(\lambda, \mu) \rightarrow \Delta m$ . Therefore, if  $\Delta m > 0$ , we have a saddle–saddle connection since for some  $0 < \mu_c < \infty$ ,  $\psi_{stable}(\lambda, \mu) - \psi_{unstable}(\lambda, \mu) = 0$ .

Thus, for an admissible phase portrait with  $\Delta m < 0$  and a non-admissible phase portrait with  $\Delta m > 0$ , saddle–saddle connections exist at finite  $\mu$ .

**Note:** The conditions  $\beta_{roots}^{\pm} = \frac{-(k_0 r_1 + k_1 r_0 + 4a_1) \pm \sqrt{(k_0 r_1 + k_1 r_0 + 4a_1)^2 - 4k_1 r_1(k_0 r_0 + 4a_0)}}{2k_1 r_1} \in (0, 1)$  can be used to check analytically if the phase portrait is admissible or nonadmissible and then the sign of  $\Delta m$  gives the necessary and sufficient conditions for a saddle–saddle connection in the system.

**APPENDIX D: CALCULATING THE CRITICAL  $\mu$**

Now, we proceed to calculate  $\mu_c$  by using a linear approximation of the saddle–saddle connection as in Ref. 13. Then, the slope of the eigenvectors at  $S_0$  and  $S_1$  will be the same as the slope of the line connecting  $S_0 - S_1$ . Then, for  $S_0$ ,

$$\left| \frac{\eta(0, m_0)}{\mu - \omega(0, m_0)} \right| = |\Delta m| \Rightarrow |\mu - \omega| = \left| \frac{\eta}{\Delta m} \right|, \tag{D1}$$



and we have  $\mu > 0$  and at  $S_0, \omega(0, m_0) = -\sqrt{r_0^2 + 4\frac{a_0 r_0}{k_0}} < 0$ . Thus,

$$|\mu + |\omega|| = \mu + |\omega| = \left| \frac{\eta}{\Delta m} \right| \Rightarrow \mu_1 = \left| \frac{\eta(0, m_0)}{\Delta m} \right| - |\omega(0, m_0)|. \quad (D2)$$

For  $S_1, \omega(1, m_1) = \sqrt{(r_0 + r_1)^2 + 4\frac{(a_0 + a_1)(r_0 + r_1)}{(k_0 + k_1)}} > 0$ , and since the Jacobian here is  $\begin{pmatrix} -\mu & 0 \\ \eta(1, N) & \omega(1, N) \end{pmatrix}$ , we have

$$|-\mu - |\omega|| = \mu + |\omega| = \left| \frac{\eta}{\Delta m} \right|, \quad (D3)$$

and therefore,

$$\mu_h = \left| \frac{\eta(1, m_1)}{\Delta m} \right| - |\omega(1, m_1)|, \quad (D4)$$

where  $\mu_1$  is the estimate at  $S_1$  and  $\mu_0$  is the estimate at  $S_0$ . Since the actual connection may not be a straight line, we average these two estimates to get a better estimate of  $\mu_c$ . Thus,

$$\mu_c = \frac{\mu_0 + \mu_1}{2} = \frac{\left| \frac{\eta(0, m_0)}{\Delta m} \right| - |\omega(0, m_0)| + \left| \frac{\eta(1, m_1)}{\Delta m} \right| - |\omega(1, m_1)|}{2}. \quad (D5)$$

Note that to prevent tipping, one must have  $\mu < \mu_c$ .

#### APPENDIX E: ALGORITHM 2: CALCULATING $\mu$ FROM DATA

1. Select two adjacent datasets and let  $t_0$  be the transition point between them and let  $N_0$  be the first value of the combined datasets.
2. We numerically integrate the differential equation  $\frac{dN}{dt} = a_0 + a_1\lambda + (r_0 + r_1\lambda)N - \frac{r_0 + r_1\lambda}{k_0 + k_1\lambda}N^2$ , where  $\lambda(t) = \frac{1}{2}(1 + \tanh(\frac{1}{2}\mu(t - t_0)))$  with the initial condition  $N_0$ .
3. Let  $N_{calc}$  be the resulting calculated value, then we calculate the loss  $L = 100 \frac{|N_{data} - N_{calc}|}{N_{data}}$ . Let the average percentage loss be  $L'$ .
4. We minimize  $L'$  over  $\mu$  to get the calculated value of  $\mu$  for the transition  $t_0$ .

Notes:

- It may be the case where  $L'$  decreases continuously with  $\mu$  without heading to a finite minimum. This happens because when the minimum is large—when  $\mu$  is large, the step function has steep growth, and therefore, the per-year sampling of the step function that we have does not have the resolution to differentiate between step functions of large  $\mu$ . In this case, we assume when the values of  $L'$  do not change much, that we have reached the actual minimum. We fix a tolerance value of  $10^{-2}$ ; i.e., when  $|L'(\mu_i) - L'(\mu_{i+1})| < Tol$ , we take  $\mu_i$  to be the calculated value.
- When numerically integrating the differential equation, the numerical solution may tend to  $-\infty$  if the value of  $\mu$  is too small. This is because the trajectory fails to fall within the stable manifold of the sink for this particular  $\mu$  and  $N_0$ . Choosing

a larger value of  $\mu$  fixes this problem. Table II contains the value of  $\mu$  calculated and the mean percentage error  $L'$  at the calculated  $\mu$ .

#### APPENDIX F: ALGORITHM 3: EXTRAPOLATION

1. Set  $\beta = Kr + 4A_0$  and calculate it.
2. If the quadratic peak of a period is almost complete (i.e., derivative decreasing and close to zero relatively), then we consider the period ended. This gives us the starting point of the period to be predicted.
3. Observe trends in  $\beta$  and  $K$  (in our data, we used linear and quadratic fits, respectively) with respect to the starting time point of that period and then estimate these values using this trend for our period. For estimating  $r$ , we fit  $r$  to an exponential model in  $K$ .
4. Use the equation  $A_0 = \frac{\beta - Kr}{4}$  to estimate  $A_0$ .
5. Use the parameters to calculate  $N$  (for  $T_{max}$ , set any value of time  $>$  starting point of period to be estimated).
6. We will vary  $r, K, T_{max}$ , and  $\beta$  (recalculate  $A_0$  each time we do so until an approximate continuity of  $N$  and  $dN/dt$  is satisfied). Changing  $K$  changes the  $N$  position of the quadratic in  $dN/dt$  vs  $N$  plot, while changing  $\beta$  changes the  $dN/dt$  position of the peak in the same plot. Changing  $r$  changes the width (change it to match other period widths), and changing  $T_{max}$  changes the  $N$  position of the predicted curve in  $t$  vs  $N$  plot. These predictions are shown in Figs. 8(e)–8(h).
7. Finally, we use  $N = \frac{1}{2}(K + \sqrt{\beta \frac{K}{r} \tanh(\frac{1}{2}\sqrt{\beta \frac{r}{K}}(t - T_{max}))})$  to calculate predictions of the growth curve [Fig. 5(b)].

Phase portraits for the transitions that occur as per our calculations in the years 1943, 1953, 1962, 1999, and 2009 are shown in Figs. 6(d)–6(h).

#### APPENDIX G: ADDITIONAL NOTES ON THE DYNAMICAL STRUCTURE OF THE SYSTEM

We have focused here on two tipping processes, but only one (the rate-induced tipping) is a bifurcation. The second is simply a threshold that approximates the boundary of the basin of the sink in the system. The bifurcation in the first process is not a local bifurcation. The system we consider always has four fixed points (one sink, one source, and two saddles) and neither their stability nor their relative configurations ever change in the processes that we consider. This bifurcation that we study is global in nature—we do not consider local bifurcations. The bifurcation occurs when the stable and unstable manifolds of the two saddles change their configuration based on the value of the parameter  $\mu$ . The intersection of the stable manifold of one saddle with the unstable manifold of the other is the bifurcation point. This is illustrated in Figs. 6(a) and 6(d)–6(h).

The combined system equations (1a) and (1b) has at most four fixed points, and we consider only this case. The stability of the fixed points and their relative positions in the phase plane undergo no change when  $\mu$  changes within a period of growth due to the fact that within a period of growth, the parameters  $r, K$ , and  $A_0$  are constant. Further, as the period of growth changes, the phase diagram may change, but the relative positions of the fixed points do not

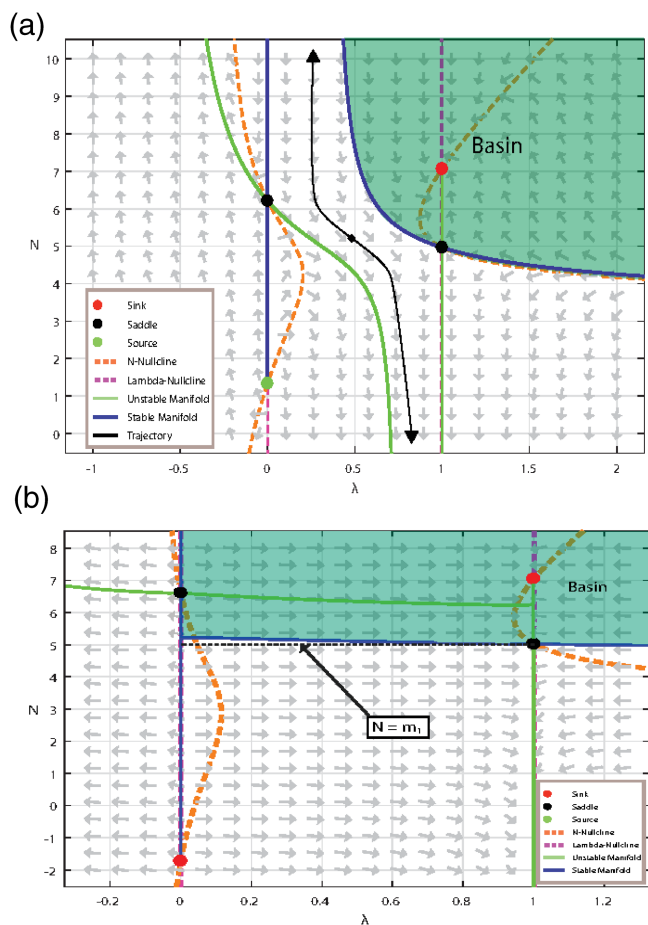


**FIG. 9.** (a) An illustration of the basin of attraction for the sink for small  $\mu$  ( $\mu = 0.10$ ). The unbounded forward and backward trajectory of an initial condition (shown as a square point) outside the basin is also shown. (b) When  $\mu$  is increased, the basin boundary is closely approximated by the line  $N = m_1$ , as shown here.

change due to the positivity restrictions imposed on  $r$  and  $K$ —i.e., the sink will always be found on the line  $\lambda = 1$  with a saddle beneath it on the same line. The source will always be found on the line  $\lambda = 0$ , with a saddle above it on the same line, etc.

The basin is not the whole space since there are saddles involved. Consider Fig. 3(a), the blue curve is the stable manifold of the saddle  $S_1$  and is the basin boundary for the attractor  $S_i$  (red). The region between the blue and green curve has trajectories that tend to  $-\infty$  in the forward direction, while tending to  $+\infty$  in the backward direction. The region bounded by the green curve is the basin for the repeller  $S_0$  (green) in the time-reversed system. This is illustrated in Fig. 9(a) for further clarity. Note that the condition  $N_{transition}$  is merely an approximation of the basin boundary. In the course of our investigations, we discovered that even if the rate-induced bifurcation occurred [which is necessary for any physically reasonable trajectory to reach the sink (we call this “growth”)], it is

not a sufficient condition for growth. For this to happen, the trajectories must start within the basin of the sink.  $\lambda$  is assumed to jump in a step fashion; therefore, the physically reasonable trajectories we consider start with  $\lambda \approx 0$ , i.e., the  $\text{CO}_2$  curve is following an approximate logistic growth model at  $\lambda \approx 0$  initially, but as  $\lambda$  ramps up, the trajectory is no longer logistic and enters into the region between the lines  $\lambda = 0$  and  $\lambda = 1$ . If the rate  $\mu$  is high enough ( $\mu > \mu_c$ ), there is a possibility that the trajectory reaches the sink—this is “growth”; otherwise, the trajectory tends to  $-\infty$ . The trajectory “grows” if and only if it begins in the basin of the sink, and in our system, the boundary of the sink can be approximated by the line  $N = m_1$  when  $m$  is large enough [see Fig. 9(b)]. The  $N_{transition}$  condition merely states whether the trajectory lies in the basin or not. There is no change in the dynamics of the system, and this is merely a condition to approximate the basin. The condition works fully when  $\mu$  is large enough. However, in the event that  $\mu$  is small but still greater than  $\mu_c$ , this condition may not ensure that growth will occur since the approximation of the boundary by the line  $N = m_1$  is poor. However, even in this case, it is guaranteed that growth will not occur if  $N < N_{transition}$ , solely because of how the boundary of the basin is related to  $\mu$ . The condition can, thus, tell if growth can be prevented but cannot always guarantee that growth will occur.

## REFERENCES

1. J. Esper, U. Buentgen, D. C. Frank, D. Nievergelt, and A. Liebhold, “1200 years of regular outbreaks in alpine insects,” *Proc. R. Soc. B* **274**, 671–679 (2007).
2. W. Baltensweiler, “Why the larch bud-moth cycle collapsed in the subalpine larch-cembra pine forests in the year 1990 for the first time since 1850,” *Oecologia* **94**, 62–66 (1993).
3. S. V. Iyengar, J. Balakrishnan, and J. Kurths, “Impact of climate change on larch budmoth cyclic outbreaks,” *Sci. Rep.* **6**, 27845 (2016).
4. P. C. Reid *et al.*, “Global impacts of the 1980s regime shift,” *Glob. Chang. Biol.* **22**, 682–703 (2016).
5. P. Friedlingstein *et al.*, “Global carbon budget 2021,” *Earth System Science Data* (published online, 2021).
6. N. A. Phillips, “The general circulation of the atmosphere: A numerical experiment,” *Q. J. R. Meteorol. Soc.* **82**(352), 123–154 (1956).
7. S. Manabe and K. Bryan, “Climate calculations with a combined ocean-atmosphere model,” *J. Atmos. Sci.* **26**, 786–789 (1969).
8. C. R. Mechoso and A. Arakawa, “General circulation—Models,” in *Encyclopedia of Atmospheric Sciences*, edited by James R. Holton (Academic Press, 2003), pp. 861–869, ISBN: 9780122270901.
9. T. M. Lenton *et al.*, “Tipping elements in the Earth’s climate system,” *Proc. Natl. Acad. Sci. U.S.A.* **105**, 1786–1793 (2008).
10. T. M. Lenton, “Early warning of climate tipping points,” *Nat. Clim. Change* **1**, 201–209 (2011).
11. P. Ashwin, S. Wicczorek, R. Vitolo, and P. Cox, “Tipping points in open systems: Bifurcation, noise-induced and rate-dependent examples in the climate system,” *Philos. Trans. R. Soc. A* **370**, 1166 (2012).
12. P. Ritchie and J. Sieber, “Early-warning indicators for rate-induced tipping,” *Chaos* **26**, 093116 (2016).
13. C. G. Perryman, “How fast is too fast? Rate-induced bifurcations in multiple time-scale systems,” Ph.D. thesis (University of Exeter, 2015).
14. N. J. Mantua and S. R. Hare, “The Pacific decadal oscillation,” *J. Oceanogr.* **58**, 35–44 (2002).
15. M. Newman *et al.*, “The Pacific decadal oscillation, revisited,” *J. Climate* **29**, 4399–4426 (2016).
16. F. P. Chavez, J. Ryan, S. E. Lluch-Cota, and C. M. Niquen, “From anchovies to sardines and back: Multidecadal change in the Pacific Ocean,” *Science* **299**, 217 (2003).

- <sup>17</sup>P. Lehodey *et al.*, “Climate variability, fish, and fisheries,” *J. Clim.* **19**, 5009–5030 (2006).
- <sup>18</sup>D. B. Irons *et al.*, “Fluctuations in circumpolar seabird populations linked to climate oscillations,” *Glob. Change Biol.* **14**, 1455–1463 (2008).
- <sup>19</sup>A. S. Sahana, S. Ghosh, A. Ganguly, and R. Murtugudde, “Shift in Indian summer monsoon onset during 1976/1977,” *Environ. Res. Lett.* **10**, 054006 (2015).
- <sup>20</sup>J. W. Dippner, K. Junker, and I. Kroencke, “Biological regime shifts and changes in predictability,” *Geophys. Res. Lett.* **37**, L24701, <https://doi.org/10.1029/2010GL045696> (2010).
- <sup>21</sup>S. Sun *et al.*, “Regime shift in the decadal variability of the Indian Ocean subsurface temperature,” *J. Mar. Syst.* **216**, 103511 (2021).
- <sup>22</sup>A. M. Powell-Xu Powell, Jr. and J. Xu, “Decadal regime shift linkage between global marine fish landings and atmospheric planetary wave forcing,” *Earth Syst. Dyn.* **6**, 125–146 (2015).
- <sup>23</sup>W. Xin-Yu, J. Zhe, and T. Ben-Kui, “Responses of planetary waves to global warming: Implications from CMIP3 4 × CO<sub>2</sub> experiments,” *Atmos. Ocean. Sci. Lett.* **6**, 109–116 (2013).
- <sup>24</sup>E. Brocard, P. Jeannot, M. Begert, G. Levrat, R. Philipona, G. Romanens, and S. C. Scherrer, “Upper air temperature trends above Switzerland 1959–2011,” *J. Geophys. Res.: Atmos.* **118**, 4303, <https://doi.org/10.1002/jgrd.50438> (2013).
- <sup>25</sup>S. N. Rodionov, “A sequential algorithm for testing climate regime shifts,” *Geophys. Res. Lett.* **31**, L09204, <https://doi.org/10.1029/2004GL019448> (2004).
- <sup>26</sup>S. N. Rodionov and J. E. Overland, “Application of a sequential regime shift detection method to the Bering Sea ecosystem,” *ICES J. Mar. Sci.* **62**, 328–332 (2005).
- <sup>27</sup>S. Khatiwala, T. Tanhua, S. E. Mikaloff Fletcher, M. Gerber, S. C. Doney, H. D. Graven, N. Gruber, G. A. McKinley, A. Murata, A. F. Rios, and C. L. Sabine, “Global ocean storage of anthropogenic carbon,” *Biogeosciences* **10**, 2169–2191 (2013).
- <sup>28</sup>T. DeVries, “The oceanic anthropogenic CO<sub>2</sub> sink: Storage, air-sea fluxes, and transports over the industrial era,” *Global Biogeochem. Cycles* **28**, 631–647 (2014).